Selective Plane Illumination Microscope dedicated to volumetric imaging in microfluidic chambers

Caroline Bissardon, Xavier Mermet, Clément Quintard, Federico Sanjuan, Yves Fouillet, Frédéric Bottausci, Marie Carriere, Florence Rivera, Pierre Blandin

Research Article Vol. 13, No. 10 / 1 Oct 2022 / Biomedical Optics Express 5261

Biomedical Optics EXPRESS

Selective plane illumination microscope dedicated to volumetric imaging in microfluidic chambers

CAROLINE BISSARDON,[1] XAVIER MERMET,[1] CLÉMENT QUINTARD,[1] FEDERICO SANJUAN,[2] YVES FOUILLET,[1] FRÉDÉRIC BOTTAUSCI,[1] MARIE CARRIERE,[3] FLORENCE RIVERA,[1] AND PIERRE BLANDIN[1,*]

[1] *Univ. Grenoble Alpes, CEA, LETI, DTBS, F-38000 Grenoble, France*
[2] *Univ. de Pau et des Pays de l'Adour, E2S UPPA, CNRS, Total, LFCR, Pau, France*
[3] *Univ. Grenoble-Alpes, CEA, CNRS, IRIG, SyMMES, F-38000 Grenoble, France*
[*] *pierre.blandin@cea.fr*

Abstract: In this article, we are presenting an original selective plane illumination fluorescence microscope dedicated to image "Organ-on-chip"-like biostructures in microfluidic chips. In order to be able to morphologically analyze volumetric samples in development at the cellular scale inside microfluidic chambers, the setup presents a compromise between relatively large field of view (~ 200 µm) and moderate resolution (~ 5 µm). The microscope is based on a simple design, built around the chip and its microfluidic environment to allow 3D imaging inside the chip. In particular, the sample remains horizontally avoiding to disturb the fluidics phenomena. The experimental setup, its optical characterization and the first volumetric images are reported.

1. Introduction

Nowadays, we observe a growing interest in tissue engineering applications, especially for organoids or organs-on-chip (OOC). Organoids are composed of various cell types that have undergone differentiation and sorted themselves to form a tissue-like ersatz [1]. Such 3D cell culture models often promote levels of cell differentiation and tissue organization that are not possible in conventional 2D cell culture systems. To reproduce *in vivo*-like conditions such as the interactions of cultured cells with circulating blood and/or immune cells, nutritive fluid flow is essential. Microfluidic OOC can be defined as "a microfluidic cell culture device that contains continuously perfused chambers inhabited by living cells arranged to simulate tissue- and organ-level physiology" [2]. OOC give the opportunity to satisfy these biological requirements for sustainable 3D cultures. Combined with microchip manufacturing, OOC support tissue structuration and mimic tissue-tissue interfaces, spatiotemporal chemical gradients, and mechanical microenvironments of organs [3]. They enable *in vitro* morphological, biochemical and bio-molecular analysis of living cells in a functional organ-like context. OOC technology makes possible to model the development and the functioning of an organ in a normal or pathological context. It enables to advance the study of tissue development and disease etiology, as well as toxicity testing and biomarker identification [2]. Moreover OOC can replace animals models [3] in the context of 3R approaches (Replacement, Reduction and Refinement, guidelines for a more ethical use of animals in testing) and open new perspectives for diagnostic and therapeutic research.

Vascularization is an important remaining challenge that must be addressed in OOC to mimic *in vivo* systems and enable nutrient delivery. Indeed, vascularization not only prevents necrosis in 3D tissue cores, but also imparts physiological morphologies and functions that involve specific adaptations to the vascular system [2]. Different methods are currently used to stimulate this nutrient exchange by generating vascular-like networks [1]. Understanding how vascularization

#455377 https://doi.org/10.1364/BOE.455377
Journal © 2022 Received 31 Jan 2022; revised 11 Apr 2022; accepted 11 Apr 2022; published 12 Sep 2022

Biomedical Optics EXPRESS

is initiated in the sample in microfluidic chamber is essential to go further in the development of OOC technology [4,5]. Many efforts are currently dedicated to addressing this challenge. For example, Schimek *et al*. [6] present a chip-based system mimicking the transport function of the human cardiovascular system. The follow-up and the imaging were realized using a two-photon microscope [6]. Techniques such as wide-field fluorescence microscopy or confocal (spinning-disk) microscopy allow global analysis of the vascular network with quantification of the length or the nodes number of the vessel network. They can also permit analysis of vessel functionality using a fluorescent beads stream. These techniques can also provide a 3D analysis of the network structure and highlight the lumen effect of capillaries. However, imaging large zones of this network with these techniques is time consuming and can induce photo-bleaching, and in the worst cases, photo-toxicity. Most of the time, these 3D studies are performed on fixed samples (sections) using an immuno-labelling and resulting in an end-point study.

Visualization and characterization of organoids and OOC are challenging since they are intermediate in size and complexity between conventional 2D cell cultures and *in vivo* organs. A valuable and interesting tool to face this challenge is light sheet fluorescence microscopy (LSFM) [7–10]. Indeed, the basic idea of LSFM consists in confining the fluorescence excitation in a plane, and acquiring the emitted fluorescence signal along an orthogonal detection path [11]. This confinement of the excitation light confers an optical sectioning capability to the microscope. Actually, compared to other imaging techniques, LSFM presents several advantages such as high-speed volumetric acquisition rate and low photo-bleaching and photo-toxicity [7,11,12] which are essential for rapid 3D imaging [13,14]. Conventional setups use a Gaussian laser beam and a cylindrical lens to generate a static light sheet. This approach is called selective plane illumination microscopy (SPIM) [10,9]. These microscopes can be easily constructed as described in the Open-SPIM platform [15]. Many configurations of LSFM have been reported [7]. Attempts to extend the field of view (FOV) without compromising Z-resolution have included the axial (i.e., along the optical axis of the excitation beam) superposition of two light sheets [16] and tiling of multiple image stacks with axially displaced light sheets [17,18]. These techniques present on the illumination and/or detection optical paths, a complex system with multiple optical elements and mechanical arrangement. In many studies, the instrument is conceived to perform analysis at high spatial resolution [19,20]. Most of these systems are large and bulky. They present a restrictive volume of analyzed sample. To achieve high quality images with the expected spatial resolution, large numerical aperture objectives immersed in index matching liquids are used. This forces the samples to be close to the objective and "optical contact" must be maintained. In many cases, organoid analyses with LSFM require sample clarification to allow visualization of the entire sample volume [21,22]. Clearing techniques are particularly used for large and thick tissue to reduce light scattering and extend the range of optical imaging. All these elements make us pretend that, in most cases, the sample must be adapted to the LSFM system used. LSFM would also be very interesting for OOC, but in this case, the setup has to be adapted to the microfluidic chip, which must perform specific functions and meet different constraints. On the other hand, LSFM presents a lot of advantages and possibilities in the field of micro-devices, as described in the detailed review by Albert-Smet *et al*. [23]. The idea of combining LSFM with fluidic devices was first given by Bruns *et al*. [24]. Some work has been done to couple and combine the chip with an adequate delivery system to customized light-sheet microscope [19] and tend to integrate optical components into a single chip [25,26]. Others have worked on generating light sheet directly in a microfluidic channel with an opto-fluidic cylindrical lens to achieve continuous imaging of cellular spheroids [27,28]. Further research has turned to the use of micro-fabricated components on a single-objective system [29–31] to achieve super-resolution on a more compact and portable device. LSFM seems to be well adapted to 3D visualization and understanding the vasculogenesis process and further general vascularization that occurs in organoid-like samples. Furthermore, this non-invasive technique allows for the

Biomedical Optics EXPRESS

follow up over time of the biological process required in these experiments while preserving the sample from photo-bleaching. As explained optical clearing enhances image quality but also generates physico-chemical modifications in the samples and distorts the purpose of the organ-on-chip investigation. For these reasons, we decided to work without optical clearing.

In this paper, we report the design, the construction and the characterization of a SPIM microscope dedicated to volumetric imaging in microfluidics chips. The main interest of this microscope is to make possible a 3D morphological and functional characterization of organoid and other tissues cultured inside a microfluidic chamber in a simple way. In particular, the setup has been designed to permit 3D characterization of complex vascularized tissues in a relatively large FOV with cellular resolution. The microscope is built around the microfluidic chip and its holder, in order to perform images inside the chip without modifying anything of its architecture or environment (connections, sample positioning. . .). In the present article, the type of microfluidic chip used and the constraints imposed on the system are presented. Then, the optical design is described and an optical characterization of the setup is reported. In a last part, the first volumetric images obtained on biological samples inside microfluidic chip are presented to attest the potential of this instrument.

2. Microfluidic chip and conception of the microscope

2.1. Constraints due to the chip

Microfluidic chips are trendy biological culture systems and present a large diversity with various sizes, geometries, and/or materials [2]. In our institute, a process flow has been defined with common manufacturing rules. The preferably used material is Cyclic Olefin Copolymer (COC), which is transparent and compatible with most of biological samples. COC also has a low level of auto-fluorescence [32], high chemical resistance [33] and low drug absorption. Moreover, it opens perspectives in terms of industrialization process [34], avoiding the complications of conventional PDMS (Polydimethylsiloxane) systems (gas permeability, incompatibility with hydrophobic compounds and adsorption of molecules) [35]. These chips have been designed to be standardized in a credit card size (85.60*53.98mm^2). In these chips, the connections are defined in the same way, with the inputs and outputs of the different fluids being positioned at the same place on the chip and with the same footprint. Depending on the application, the precise architecture of the channels and chambers in the chip can be modified. The chambers can be easily adapted to the study and the samples (concentration, dilution, species separation, labeling, lysis, biomechanics . . .). Although the primary objective of the device is to study vascularization mechanisms in specific architectures, the setup can be used on many other chips manufactured in our department.

Conventionally, COC possesses acceptable optical quality for classical transmission imaging, but the thickness of the cover of usual microfluidic chips is quite important (typically 1 up to 3mm) and there may be surface defects (flatness and roughness). Because of these issues and to reduce the impact of this material on image quality, in the present setup we replaced one of the walls of the microfluidic chip by a thin 150µm-thick polypropylene film. We also chose to excite and detect the fluorescence through this same surface of better optical quality. This substitution of one side of the chip (thinner wall) will helps preserving both the excitation confinement and the image quality by less optical scattering. The mechanical dimensions of the chip, the microfluidic environment and the required angles between the excitation and detection optical axes in the SPIM configuration [7], do not allow to work with the conventional objectives used in LSFM. The objective cannot be placed very close to the sample. To face this problem, a long working distance objective is required.

Furthermore, in order to limit potential environmental disturbances in the sample development and to avoid any microfluidic injection problem, the microfluidic chip has to be analyzed horizontally. Consequently, in the present setup, the illumination and imaging of the sample are

Biomedical Optics EXPRESS

carried out from the upper side of the microfluidic chip where is the thinner wall composed of glass or polypropylene film. This requires mounting the optical system on a vertical breadboard (see Fig. 1).

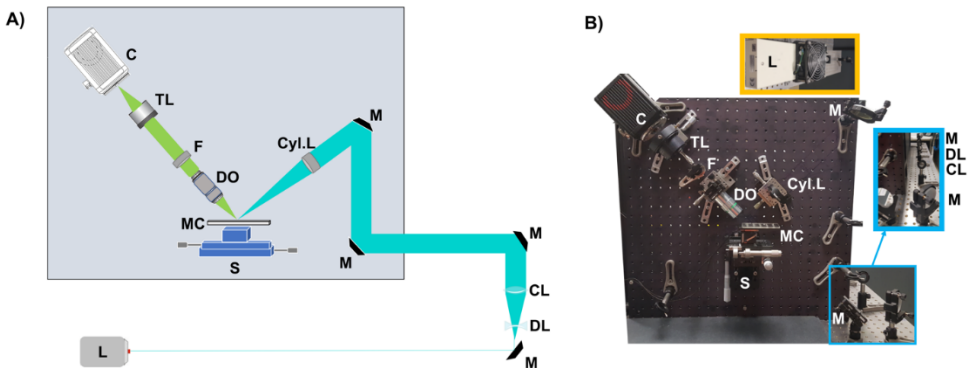

Fig. 1. Experimental set-up with L: laser, M: Mirror, DL: Diverging Lens, CL: Converging Lens, Cyl.L: Cylindrical Lens, MC: Microfluidic Chip, S: (manual & computed-controlled) micromertric stages, DO: Detection Objective, F: Filter, TL: Tube Lens, C: sCMOS Camera. A) Simplified sketch of the SPIM. B) Picture of the real set-up with in inserts: the yellow rectangle for the view of the laser source placed just behind the breadboard, and the blue rectangles for the view of the afocal system to enlarge the laser beam.

To follow the vascularization process, the microfluidic architecture associated with an adequate microfluidic injection system has been developed in our department. The design of the microfluidic chip has been thought to optimize the perfusion system on vascularization initiation method. Different microfluidic chips designed in our department with significantly different chamber architectures have been tested and validate this microscope configuration. Even though our microscope is designed to be used for a chip format with different chamber configurations and various samples, we expect the overall imaging performances to be highly dependent from the diverse components (liquid, tissues, proteins . . .) present in the channels of the microfluidic chip. Light absorption and scattering will be different, especially as we do not clarify the samples. As known in LSFM, these phenomena might considerably reduce the performances.

Finally, unlike other systems focused on super-resolution or on large field of view imaging, the main purpose of this instrument is to obtain the best compromise between a volume study on large areas of a few mm^2 and a cellular resolution to highlight the lumen in the capillaries. This will provide a morphological and functional analysis of the vascularization process in 3D.

2.2. Optical design

We developed a SPIM system adapted to the sample position. It was conceived in a way that minimize as possible the handling of optical elements and the sample. A sketch is presented in Fig. 2(A). From this figure it can be seen that to meet the constraints of microfluidic and sample study, our microscope was designed to observe the sample at 45 degrees respect to its horizontal position. Wu *et al*. [36] developed an inverted selective plane illumination microscope (iSPIM) that allows the sample to be positioned horizontally. Thus, our system mimics this same configuration which already showed its good potential [37]. However, in our case we used a long working distance objective. Indeed, due to the 45° angle, to image a sample positioned 500µm in depth regarding the chip surface, the minimum working distance required is 700 µm. Since the objective cannot enter inside the chip, we must take into account its physical size: and for an objective entrance diameter of 10 mm, we need 5 mm to reject the objective outside the fluidic chamber. So we need a working distance longer than 5.7 mm.

Biomedical Optics EXPRESS

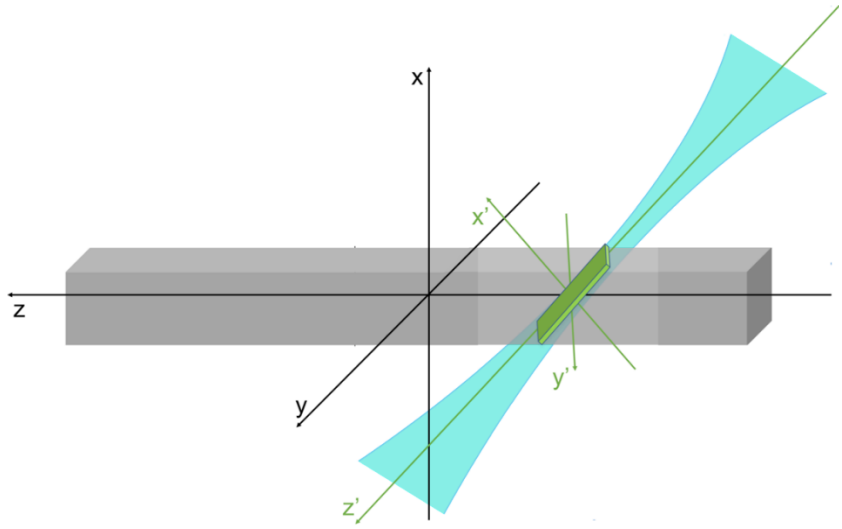

Fig. 2. Scheme of the reference systems: the xyz system of the microfluidic chip (black basis) and the x'y'z' system of the illuminated section (green basis).

Based on the Open-SPIM platform [15,38] and considering the constraints imposed by the microfluidic chip system, we selected the optical elements for our experimental setup. In particular, we fixed that the microscope should have a spatial resolution of a few µm (< 5µm) to study vascularization, and a FOV of several hundred µm, since the studied samples can extend up to a few mm.

During development we focused first on the excitation path, i.e. the light sheet generation. The thickness of the light sheet (LS) determines the microscope axial resolution and FOV. A thinner LS causes a FOV reduction, resulting in a trade-off that is determined by the Gaussian laws of beam propagation. Therefore, twice the Rayleigh length (Z_R) is usually considered as the distance over which the axial resolution is kept in the excitation propagation direction. $Z_R = \frac{\pi w_0^2}{\lambda}$, where w_0 is the waist radius and λ the wavelength. This distance corresponds to a beam width lower or equal to $\sqrt{2}w_0$, and is used in this paper to define the FOV size in the excitation propagation direction. The excitation beam propagates through the air and after the lens, it crosses the microfluidic chip oriented at 45 degrees from the optical axis. Theoretically, by using a beam expanded with a diameter of 15mm before being focused with a 100mm focal length cylindrical lens, we expect to obtain a waist diameter of approximatively 4,14µm (considering a wavelength of 488 nm) and an axially confined illumination field of approximatively 221µm ($2Z_R$).

Secondly, we investigated the imaging path. We first chose the magnification factor. Considering a sensor with a pixel size of 6.5µm and square area of 13.3mm side, a magnification of 10 will offer a good spatial sampling, close to the Shannon-Nyquist criteria, and will give access to an imaged area of approximatively 1mm^2 in the object plane. This value covers the spatial extension of the light sheet and also the diameter of the microfluidic channel of interest. In our laboratory we already had the 20x super long working distance objective from Mitutoyo (M Plan Apo SL 20x, WD = 30.5 mm, NA = 0.28), so we decided to use it but associated with a tube lens with shorter focal length than the 200mm recommended by Mitutoyo. This way we can adjust the magnification with still a long working distance and a good numerical aperture (NA). To guarantee a magnification of about 10, we checked that a 100mm focal length tube lens is adequate and compatible with the objective we chose. Theoretically, the lateral resolution r can be given by the radius of Airy disk: $r = 0.61\frac{\lambda}{NA}$, with λ the fluorescence emission wavelength and NA

Biomedical Optics EXPRESS

the numerical aperture. In our case, with a fluorescence emission at 520nm (Green Florescence Protein, GFP or Fluorescein) and NA = 0.28, we obtain $r = 1.13\mu m$, which is in agreement with the expected optical performances. In this part, we didn't consider the astigmatism and other potential optical aberrations due to the 45 degrees angle between the chip and the imaging optical axis.

2.3. Description of the optical experimental set-up

The beam is emitted by an Argon ion Air-cooled laser systems (Spectra Physics488nm, 10mW max). Using a beam analyzer (BC106N-VIS, Thorlabs), we measured a full width half-maximum (FWHM) value of 760µm for the Gaussian-like shape laser core. Several iris diaphragms (ID20/M Thorlabs,) have been placed all along the optical path to properly define the optical axis. As depicted in Fig. 1, the beam is redirected by an one-inch mirror (BB1-E02 Thorlabs), expanded and collimated by an afocal system with a magnification factor of 16, formed by a -25mm focal length diverging lens (LC1054-A Thorlabs) and a 400mm focal length converging lens (LA1172-A Thorlabs). The resulting collimated beam has a total extension about 23mm. For the experiments, we used the central and homogeneous part of the extended beam with a size of 13mm (corresponding to the FWHM intensity profile of the total extended beam). In the sketch (Fig. 1), we can notice that the illumination and detection paths are in vertical position. The laser beam is thus oriented in a vertical plane with an incident angle of 45 degrees with respect to the chip holder using three two-inch mirrors (BB2-E02 Thorlabs). The light sheet is generated by a 100 mm focal length cylindrical lens (LJ1567RM-A Thorlabs). This optical element allows to form a fine and homogeneous light sheet on the field of view of the camera. The 3D imaging is then possible by translating the sample, keeping the LS static. The fluorescence signal generated at the illuminated plane is collected by an infinite corrected long working distance objective lens (OL) (20X Mitutoyo Plan Apo SL, Mitutoyo, 20x, NA: 0.28, WD: 30.5mm). In Fig. 2, two reference axis systems are defined: (i) the base of the microfluidic chip (xyz) and (ii) the base of the light sheet (x'y'z'). The detection optical axis, x', is orthogonal to the excitation optical axis z', and approximately 45 degrees from the z direction of the chip holder. The cylindrical and objective lenses are placed on stages in order to position the illumination sheet in the plane of interest at the expected depth in the sample, and also to be able to adjust the focus of the objective. The 20x Mitutoyo objective has been then combined with a 100mm-tube lens (TTL100-A Thorlabs) as previously explained to reach a magnification factor close to 10. The tube lens is used to form the image of the fluorescent structure onto a high-sensitive sCMOS camera (HPF ORCA FLASH 4.0V3-Pack, Hamamatsu). To filter out the laser excitation, an interference filter (BLP01-488R-25 Semrock) is mounted on an extension fixed to the objective lens holder. The sample is mounted on a custom-designed holder attached to a computer-controlled linear xz translation stages (ECSx3030/AI/NUM/RT Attocube and ECSz3030/AI/NUM/RT Attocube). A control unit is used to coordinate the movement of these stages (AMC100/NUM Attocube). The sample displacement can thus be controlled at the micrometer scale. A 3-axis rollerblock long-travel bearing stage (RB13M/M Thorlabs) is also used to pre-position the area of interest of the microfluidic chip in the optical axis, and to access the entire sample present on our specific microfluidic chip. Once everything is perfectly aligned, moving the chip by the computer-controlled stages allows the acquisition of a collection of images.

The camera and the computer-controlled stages are driven by a LabVIEW (National Instruments) program. This program allows to synchronize the movement of the sample with the images capture in TIFF format. Worth to mention that the configuration we used have been thought to allow the three directional motions of the chip. The 3D imaging is then possible thanks to the translation of the chip, permitting a relative displacement of the sheet at different depths and transverse positions of the sample.

Biomedical Optics EXPRESS

3. Results

3.1. System characterization

First, we characterized the LS in air by imaging the transverse intensity distribution in different planes along the beam propagation direction. This characterization seemed important to us before working in the chip, because the thickness and uniformity of the LS strongly impact the image quality. Using the reference system described in Fig. 2, the lateral extension of the static light sheet was about 13mm in the y' direction. The beam extension was limited by the mounted optical supports present along the propagation. From our measurements, we estimated that over a propagation distance of 150µm around the focal plane, the LS had a thickness of 15µm or less and over 500µm of propagation distance, it had a thickness of at most 25µm.

To achieve the magnification factor we performed measurements with a fluorescent 1951 USAF resolution test chart. We obtained a magnification of 12. Then, the size of the total imaged area of the sample on the sCMOS, regardless of the light sheet thickness and the optical sectioning, was measured as ~ 12.9mm*12.9mm.

As well described in conventional LSFM, the axial resolution is related to the light sheet thickness and the lateral resolution to the optics used for imaging [7,23,39].With the selected properties of the objective used, as explained previously, the theoretical transverse resolution value r due to diffraction limit is 1,13µm. The theoretical axial resolution can be defined by the half-length of the PSF in the axial direction [7] $R_{det-axial} = \frac{1.78.n.\lambda_{em}}{NA_{det}^2}$ is equal to 14.7µm for n = 1.33.

The system was optically characterized in a conventional manner using fluorescent yellow-green 500nm beads (Thermofischer scientific, G500). These specific nanoscale beads, smaller than the resolution expected by the diffraction limit, permit to study point spread function (PSF) of our system. These microbeads diluted in a gel solution were injected into the microfluidic system. After gel reticulation, the beads were imaged, with the light sheet adjusted so that the thinnest part was located close to the top of the chamber. Figure 3 shows the z'y' plane of the selected region of interest (ROI). A collection of normalized PSF on on-focus and individualized beads was made over 30 measurements to be statistically accurate. FWHM values were then obtained using a Gaussian fit for each profile and yielded a mean ± SD (SD = standard deviation) value of $d_{FWHM} = 5.2 \pm 1.1$µm. Using the formula $resolution = 1.19.FWHM(PSF)$ given by Born&Wolf [40], the lateral resolution was then about 6.2 ± 1.3µm. As expected, the sizes of the images of the beads trapped in the gel in the microfluidic chamber (Fig. 3) were larger than those of the same beads laid on a glass microscope slide ($d_{FWHM} = 1.6 \pm 0.2$µm for a resolution of 1.9 ± 0.2µm). This can be explained by the additional aberrations introduced by the use of a long working distance air objective for imaging aqueous samples. Moreover, the 45 degree tilted air-chip interface adds aberration in the z' direction: the PSF in the plane of the light sheet is more extended in the z' direction (Fig. 3(A)). The proposed Gaussian fit doesn't take it into account, so in this direction, the resolution can be considered lower than the reported mean value.

The axial resolution $R_{det-axial}$ was also investigated in order to define which of the objective or the light sheet limits the resolution. Intensity profiles of the same beads were measured by moving the objective along x' direction (optical axis of detection) in different positions (10 positions spaced 5µm apart) without modifying the light sheet. The depth of field (DOF) was about $d_{FWHM} = 20 \pm 1.2$µm. Then, we fixed the objective and the light sheet and we measured the normalized intensity profiles of several beads on the x'z' plane by translating the sample in the x' direction with 1µm step size (30 beads measurements to be meaningful). FWHM values were obtained using a fit for each profile and provided a mean ± SD value of $d_{FWHM} = 18.8 \pm 2.3$µm. Here again, due to additional aberrations, this value was higher than the one obtained with the beads laid on the glass slide: 15.1 ± 1.4µm. This means that the optical sectioning comes from

Biomedical Optics EXPRESS

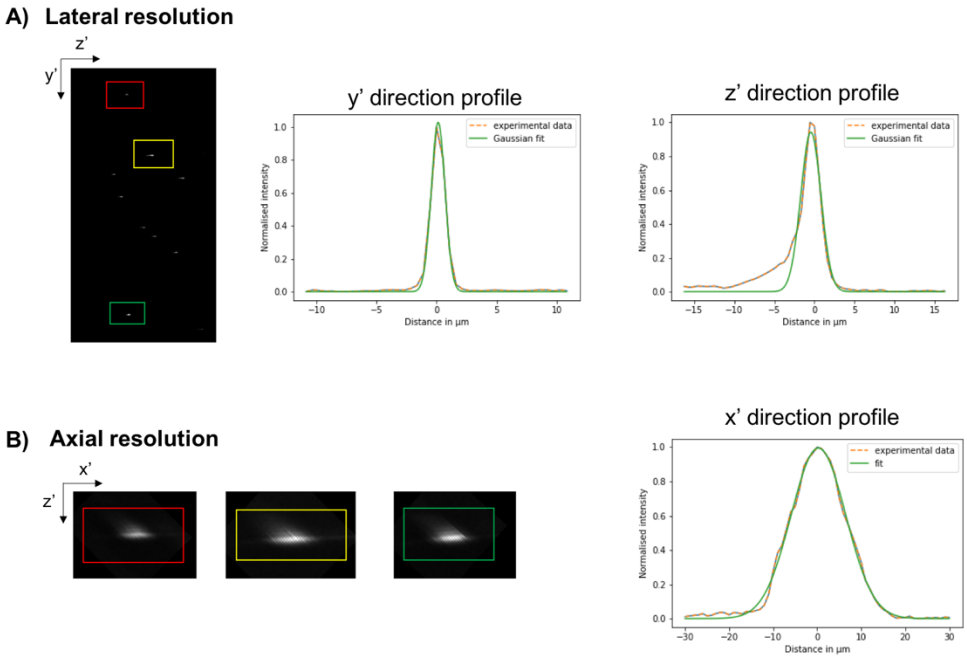

Fig. 3. A) z'y' plane of the selected ROI and corresponding intensity profiles of the PSF along z'- and y'-direction with the fitted Gaussian curve associated for 500nm fluorescent bead embedded in hydrogel. B) z'x' plane of the selected ROI and corresponding intensity profiles of the PSF along x'-direction.

the light sheet itself and it is not limited by the objective; the axial resolution is then well defined by the light sheet thickness.

Considering this time the optical sectioning due to the light sheet, we obtained an effective FOV of 150µm*12.9mm.

3.2. Imaging organoids inside microfluidic chamber

In vitro organ-on-chip experiments were performed. We wanted to image over time the initiation and development of the vascular network induced by the differentiation of a mesenchymal organoid made of fibroblasts and endothelial cells. The endothelial cells (HUVEC) of the organoid expressed green fluorescent protein (GFP). The organoid was embedded in a fibrin hydrogel, loaded into the chip and trapped in a U-cup shaped predefined location. The design of the spheroid trap in the chip is reported Fig. 4. The GFP-HUVEC cells self-organized into a three-dimensional microvascular network after a few days. We imaged directly in the microfluidic chamber the expansion of the GFP-HUVEC cells every two days over a period of 10 days. For each imaging session, the chip was removed from the incubator and positioned on the dedicated microscope holder. The LS position and focus were readjusted to image properly the sample. Fluorescence images were then acquired in different planes spaced at 5 µm along the microfluidic channel. These planes we obtained by translating the chip. The travel of the translation stage gives the maximum length of the channel that can be imaged: here, 20 mm. The image processing performed to obtain the 3D volumes is presented in appendix.

Figure 5 presents a 3D rendering of a newly formed microvascular network after 8 days of culture in a microfluidic system. Figure 5(B) shows a 360° view of the capillaries newly developed around and within the organoid. Figure 5(A) was obtained with a conventional inverted fluorescence microscope used for control and provides a 2D image of the projection of all

Biomedical Optics EXPRESS

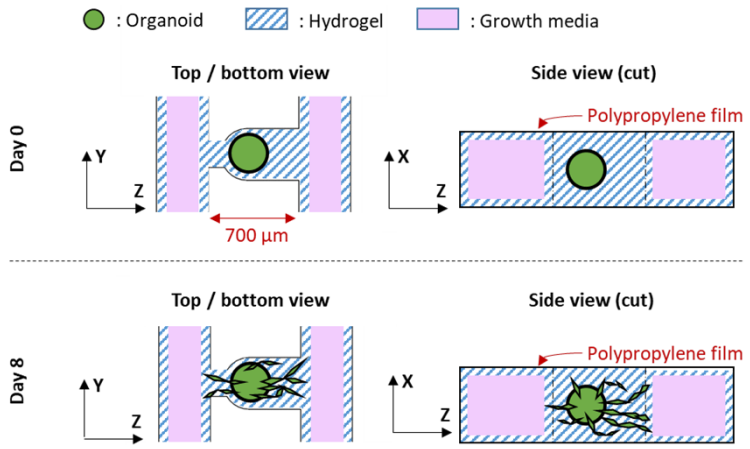

Fig. 4. Scheme of the U-cup shaped trap containing the organoid. Hydrogel is distributed on the edges of the microfluidic channels and in the trap, and the channels are filled with growth media to promote the development of the vascular network. The orientation axis defined in Fig. 2 are reported.

fluorescent cells present in the chip forming the global vascular network. With our optical system and a simple data analysis (thresholding and 3D viewer software), we were able to visualize the tortuosity and the size of the capillaries.

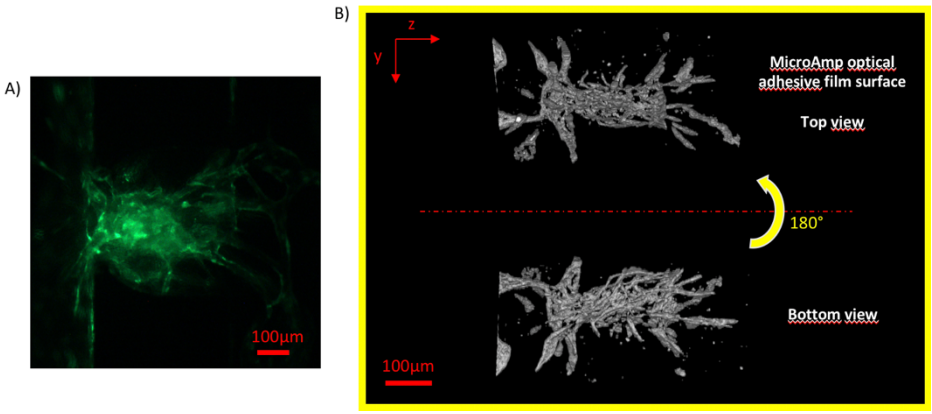

Fig. 5. A) Inverted fluorescence microscope image that provides a 2D image of the projection of all fluorescent cells present on the chip forming a global vascular network after 8 days culture. B) 3D rendering of the same vascular network obtained from 170 planes images with the light sheet (z is the direction of the stage displacement). The orientation axis defined in Fig. 2 are reported. The images correspond to the Top / Bottom view of Fig. 4.

As previously explained, with our setup, the same sample contained inside a microfluidic chip can be repositioned for daily observation. Figure 6 illustrates this property by reporting 3D rendering of the same area of the same vascular network after respectively 1 day, 4 days, 6 days and 8 days of culture. After 1 day, the cells occupy a sphere as during the trapping of the organoid; there is no evidence of network development. From the 4th day, we clearly see that the cells self-organize into a three-dimensional microvascular network. After 6 and 8 days, vessels become distinguishable, and the spatial extent of the network and its complexity increase. These images make it possible to consider the quantitative three-dimensional study of the development

Biomedical Optics EXPRESS

of the vascular network, by measuring for example the density or the length of the network, or estimating the number of nodes. Such a study requires advanced image processing steps that have not been performed in the framework of the work reported here.

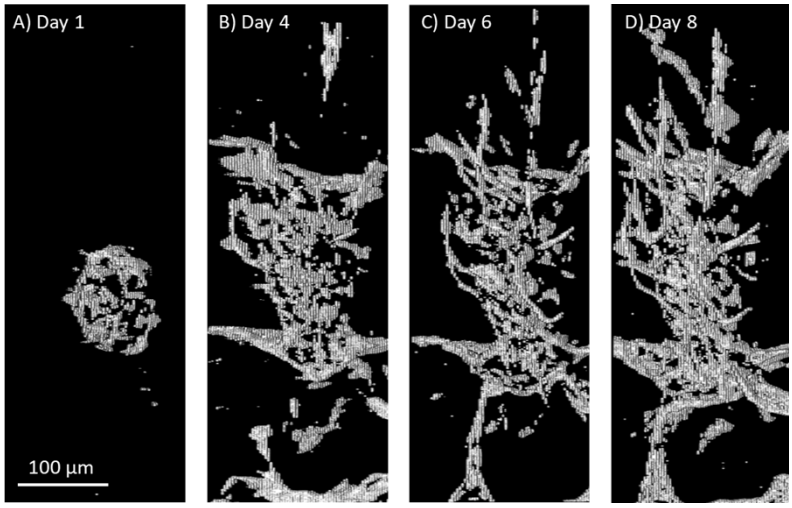

Fig. 6. 3D rendering of the same area of the same vascular network over time. A) After 1 day of culture (100 planes images). B) After 4 days of culture (crop, 247 planes images). C) After 6 days (152 planes images). D) After 8 days (170 planes images).

4. Discussion and perspectives

Vascularization is a key point in OOC technology and it requires to be studied without any chemical- or photo-degradation. The need of an instrument allowing the 3D follow-up and rapid imaging inside microfluidic chip is then crucial. The original SPIM setup we present here can help solve these burning issues. With our new imaging setup, we are able to easily visualize the organoid and its differentiation into a vascular network directly in the microfluidic chamber. A follow-up of the vascularization can be done over time (several days) without any impact on the cell proliferation. As presented, we acquired images on the same sample every two days over 10 days to establish the characterization of the vascularization of the organoid cultured in the microfluidic chamber. Depending on the needs of the experiments, we are able to image the sample in the microfluidic chamber over a 20 mm large zone with a resolution suitable for the distinction of the newly formed vascular structures. As far we know, our instrument is the only system able to achieve such performances. This first prototype of our system presents some performance limitations. The light sheet confinement is degraded by the polypropylene film used to seal the microfluidic chamber and the hydrogel that constitutes the cellular scaffold in the chip. This directly impacts the axial resolution, especially in the deeper part of the microfluid channel, in the region with the larger cell density, where the excitation is not homogeneously distributed. Furthermore, the refraction angles also impact the microscope performances: in this setup, the image plane conjugated to the detection plane is not perfectly parallel to the light sheet plane. This generates a blur in some region of the acquired images.

This non-invasive technique used with this experimental setup allows a long-term follow-up of the biological process. The main interest of this microscope is to allow a 3D morphological and functional characterization of hydrated biological samples that are continuously perfused in a microfluidic chamber. Thanks to the detailed characterization reported here, we are convinced that the performance of our system is interesting to follow the vascularization process inside

Biomedical Optics EXPRESS

a microfluidic chamber. An estimation has been made and the sample information have to be acquired in a reasonable time frame e.g. between 1 and 4 2D-images per sec. In order to limit any modification of external factors, an investigation for a complete automation of the experimental setup to reduce the total acquisition time is under investigation.

We keep in mind that this first implementation is the simplest one, and confronted to real thick biological samples, the performance is somewhat degraded. The challenge will be to optimize the microscope while preserving a simple and versatile configuration able to work with different chip designs in microfluidics laboratory. Scattering inside the sample degrades the confinement of the light sheet during its propagation. This phenomenon will strongly depend on the observed sample. Thus the field of view, i.e. the area over which the thickness of the light sheet remains compatible with the desired axial resolution, is also reduced. This can be combated by translating the light sheet and consequently the waist position in the propagation direction, and by synchronizing it with the rolling shutter of the CMOS camera to confocal-like detect the fluorescence line by line, as reported previously [41–43]. Another solution is to use a digital scanning light-sheet process, with Airy or Bessel-type beam shaping to limit expansion during the propagation [19,13–46]. It may also be necessary to optimize the translation of the sample along the optical axis allowing for scanning the detection path [47], slightly tiling of the illumination [19,48], engineering of the detection point spread function [17,49] or modulating the light in the perpendicular direction. In addition, the light propagates inside the chip material in a rotation asymmetric way, due to the 45-degree incident angle on the chip, inducing optical aberrations. One solution could be to numerically correct this aberration, for example by deconvolving the measured PSF in the entire FOV. Another solution could be to add a prism to ensure that the excitation and detection optical axis are normal to the interface [50], or to use a deformable mirror [51].

Regarding the actual angle between the excitation and detection paths, the setup has been designed on a 90 degrees angle at the surface of the microfluidic chip. Analyses inside the chamber highlight an angle issue that decrease the image quality of the sample. The focal plane of the light sheet is not perfectly perpendicular to the detection path, which locally affects the image quality. If we restrict the sample analysis just below the surface of the material closing the microfluidic chamber, it is possible to obtain results with little degradation of the image quality, as illustrated Fig. 4. However, when analyzing samples located deeper in the microfluidic chamber, for example at the bottom of the chamber, light will face to the different refractive index of the materials and the image quality will be significantly diminished. Considering a chamber filled with water or hydrogel, this configuration creates a definitive angle within the chamber of about 65 degrees, independently on the material used for the chip. Once again, depending on the expected performances for a given sample, a next step for this prototype could be to modify the angle configuration to precisely obtain the 90 degree angle in the chamber. In our case, 140 degrees might be required between the illumination and detection paths. However, it is very difficult to conjugate such large angle configuration with a large and complex microfluidic system. Mechanically, the motion of the chip to examine the entire chamber will be restricted. A prism [50] or a hemispherical solid-immersion lens [14] can also be a solution to reduce this angle between these two optical arms.

5. Conclusion

In this manuscript, we report the design and the realization of an original SPIM dedicated to study the vascularization in microfluidic chip. This system, based on a light sheet generated by a cylindrical lens and a detection using long working distance objective is able to perform imaging inside any chamber of microfluidic chips manufactured in our institute. These chips were fabricated with similar materials (COC, sealing with polypropylene) but with completely different chamber architectures. With our light sheet fluorescence microscope we can perform both (i) a volume study over quite large zones with sufficient resolution to highlight the lumen

Biomedical Optics EXPRESS

in the capillaries and (ii) a microfluidic study over time, 5 min or less being needed to image in 3D the whole microfluidic chamber of the chip. The sample can then be analyzed under perfusion or not and placed directly back into the incubator after imaging. We characterized the performances of the first implementation of this setup. This microscope reaches a lateral resolution about 6.4µm and an axial resolution of 22.4µm in a FOV of 150µm*12.9mm^2 inside a microfluidic chamber. With a fixed illumination and detection system, the sample contained in the microfluidic chamber is then imaged by controlled-stages motions of the chip. The acquired images can be then directly used to visualize the sample in 3D. These 3D renderings already provide some useful and significant parameters for understanding the vascularization process of organoids. We expect that the further study of continuously perfused complex biological samples will degrade performance, and some optimizations are proposed to be able to follow what is happening in these chambers.

Appendix A

A.1 Fluorescent microbeads sample preparation

500nm mean particle size fluorescent microbeads (Latex beads, carboxylate-modified polystyrene, fluorescent yellow-green, aqueous suspension: Thermo-fischer scientific G500 – 500nµm) were diluted at 1:10000 in ddH2O and pipette on a classic microscope slice (Thermo scientific Menzel-Gläser microscope slides, ground edged slides are 75mm x 25mm and 1 mm thick). Beads were suspended into an aqueous solution (containing mainly ddH2O) or a hydrogel depending on the experiment. The hydrogel was made of 6.6mg/mL fibrinogen, 0.15TIU/mL aprotinin, 2.5mM CaCl2 and 1U/mL thrombin prepared in HEPES-buffered saline (Sigma–Aldrich, Taufkirchen, Germany). It is expected to have a ratio of 1.8 beads per µL. 20µL of one of these preparations were pipetted into the microfluidic channel. The microfluidic chip was sealed with a MicroAmp optical adhesive film (Thermo Scientific 4311971) to avoid evaporation. The chip was left at room temperature for 15 minutes to allow polymerization of the hydrogel.

A.2 Data analysis

The PSF were obtained by a simple Python script. We plotted the normalized intensity (AU) vs the distance in µm. Then we used a Gaussian fit to extract the FWHM of the curve that provides the PSF.

The acquired 2D images are analyzed by batch. The individual images are normalized in order to remove of the background noise. To obtain 3D rendering, a Bradley local image thresholding using Matlab is performed (threshold: 0.41, window size: 201 pixels) for each individual images. The volume presented were obtained by opening the stack thus created with 3D plugin of ImageJ.

Funding. Commissariat à l'Énergie Atomique et aux Énergies Alternatives.

Acknowledgments. The authors thank O. Cioni and Dr. E. Brun for their scientific exchanges about data analysis and 3D-reconstruction and Dr. E. Bergmann for the exchanges about the development of the automated system of the camera and the stages.

The authors acknowledge the financial support of the Transversal Instrumentation and Detection Program of the CEA, the French Atomic Energy and Alternative Energy Commission.

Disclosures. The authors declare no conflicts of interest.

Data availability. Data underlying the results presented in this paper may be obtained from the authors upon reasonable request.

References

1. M. A. Lancaster and J. A. Knoblich, "Organogenesisin a dish: Modeling development and disease using organoid technologies," Science **80**, 345 (2014).
2. S. N. Bhatia and D. E. Ingber, "Microfluidic organs-on-chips," Nat. Biotechnol. **32**(8), 760–772 (2014).
3. D. Huh, G. A. Hamilton, and D. E. Ingber, "From 3D cell culture to organs-on-chips," Trends Cell Biol. **21**(12), 745–754 (2011).

Biomedical Optics EXPRESS

4. K. Haase and R. D. Kamm, "Advances in on-chip vascularization," Regen. Med. **12**(3), 285–302 (2017).
5. Y. Nashimoto, R. Okada, S. Hanada, Y. Arima, K. Nishiyama, T. Miura, and R. Yokokawa, "Vascularized cancer on a chip: The effect of perfusion on growth and drug delivery of tumor spheroid," Biomaterials **229**, 119547 (2020).
6. K. Schimek, M. Busek, S. Brincker, B. Groth, S. Hoffmann, R. Lauster, G. Lindner, A. Lorenz, U. Menzel, F. Sonntag, H. Walles, U. Marx, and R. Horland, "Integrating biological vasculature into a multi-organ-chip microsystem," Lab Chip **13**(18), 3588–3598 (2013).
7. O. E. Olarte, J. Andilla, E. J. Gualda, and P. Loza-Alvarez, "Light-sheet microscopy: a tutorial," Adv. Opt. Photonics **10**(1), 111 (2018).
8. A. Mittone, I. Manakov, L. Broche, C. Jarnias, P. Coan, and A. Bravin, "Characterization of a sCMOS-based high-resolution imaging system," J. Synchrotron Radiat. **24**(6), 1226–1236 (2017).
9. M. Weber and J. Huisken, "Light sheet microscopy for real-time developmental biology," Curr. Opin. Genet. Dev. **21**, 566–572 (2011).
10. J. Huisken and D. Y. R. Stainier, "Selective plane illumination microscopy techniques in developmental biology," Development **136**(12), 1963–1975 (2009).
11. J. Huisken, J. Swoger, F. Del Bene, J. Wittbrodt, and E. H. K. Stelzer, "Optical sectioning deep inside live embryos by selective plane illumination microscopy," Science **305**(5686), 1007–1009 (2004).
12. L. A. Royer, W. C. Lemon, R. K. Chhetri, Y. Wan, M. Coleman, E. W. Myers, and P. J. Keller, "Adaptive light-sheet microscopy for long-term, high-resolution imaging in living organisms," Nat. Biotechnol. **34**(12), 1267–1278 (2016).
13. F. O. Fahrbach, F. F. Voigt, B. Schmid, F. Helmchen, and J. Huisken, "Rapid 3D light-sheet microscopy with a tunable lens," Opt. Express **21**(18), 21010 (2013).
14. A. K. Glaser, N. P. Reder, Y. Chen, E. F. McCarty, C. Yin, L. Wei, Y. Wang, L. D. True, and J. T. C. Liu, "Light-sheet microscopy for slide-free non-destructive pathology of large clinical specimens," Nat. Biomed. Eng. **1**, 1–10 (2017).
15. P. G. Pitrone, J. Schindelin, L. Stuyvenberg, S. Preibisch, M. Weber, K. W. Eliceiri, J. Huisken, and P. Tomancak, "OpenSPIM: an open-access light-sheet microscopy platform," Nat. Methods **10**(7), 598–599 (2013).
16. R. Tomer, K. Khairy, F. Amat, and P. J. Keller, "Quantitative high-speed imaging of entire developing embryos with simultaneous multiview light-sheet microscopy," Nat. Methods **9**(7), 755–763 (2012).
17. K. M. Dean, P. Roudot, E. S. Welf, G. Danuser, and R. Fiolka, "Deconvolution-free subcellular imaging with axially swept light sheet microscopy," Biophys. J. **108**(12), 2807–2815 (2015).
18. L. Gao, "Extend the field of view of selective plan illumination microscopy by tiling the excitation light sheet," Opt. Express **23**(5), 6102–6111 (2015).
19. R. Regmi, K. Mohan, and P. P. Mondal, "High resolution light-sheet based high-throughput imaging cytometry system enables visualization of intra-cellular organelles," AIP Adv. **4**(9), 097125 (2014).
20. L. K. Chin, C.-H. Lee, and B.-C. Chen, "Imaging live cells at high spatiotemporal resolution for lab-on-a-chip applications," Lab Chip **16**(11), 2014–2024 (2016).
21. Y. Y. Chen, P. N. Silva, A. M. Syed, S. Sindhwani, J. V Rocheleau, and W. C. W. Chan, "Clarifying intact 3D tissues on a microfluidic chip for high-throughput structural analysis," Proc. Natl. Acad. Sci. **113**(52), 14915–14920 (2016).
22. K. Chung and K. Deisseroth, "CLARITY for mapping the nervous system," Nat. Methods **10**(6), 508–513 (2013).
23. I. Albert-Smet, A. Marcos-Vidal, J. J. Vaquero, M. Desco, A. Muñoz-Barrutia, and J. Ripoll, "Applications of Light-Sheet Microscopy in Microdevices," Front. Neuroanat. **13**, 1 (2019).
24. T. Bruns, S. Schickinger, R. Wittig, and H. Schneckenburger, "Preparation strategy and illumination of three-dimensional cell cultures in light sheet–based fluorescence microscopy," J. Biomed. Opt. **17**(10), 1015181 (2012).
25. H. Deschout, K. Raemdonck, S. Stremersch, P. Maoddi, G. Mernier, P. Renaud, S. Jiguet, A. Hendrix, M. Bracke, R. Van Den Broecke, M. Röding, M. Rudemo, J. Demeester, S. C. De Smedt, F. Strubbe, K. Neyts, and K. Braeckmans, "On-chip light sheet illumination enables diagnostic size and concentration measurements of membrane vesicles in biofluids," Nanoscale **6**(3), 1741–1747 (2014).
26. P. Paiè, F. Bragheri, A. Bassi, and R. Osellame, "Selective plane illumination microscopy on a chip," Lab Chip **16**(9), 1556–1560 (2016).
27. P. Paiè, F. Bragheri, T. Claude, and R. Osellame, "Optofluidic light modulator integrated in lab-on-a-chip," Opt. Express **25**(7), 7313–7323 (2017).
28. P. Paiè, R. Martínez Vázquez, R. Osellame, F. Bragheri, and A. Bassi, "Microfluidic based optical microscopes on chip: microscopes on chip," Cytom. Part A **93**(10), 987–996 (2018).
29. E. Zagato, T. Brans, S. Verstuyft, D. van Thourhout, J. Missinne, G. van Steenberge, J. Demeester, S. De Smedt, K. Remaut, K. Neyts, and K. Braeckmans, "Microfabricated devices for single objective single plane illumination microscopy (SoSPIM)," Opt. Express **25**(3), 1732 (2017).
30. Z. Elisa, B. Toon, S. C. De Smedt, R. Katrien, N. Kristiaan, and B. Kevin, "Technical implementations of light sheet microscopy," Microsc. Res. Tech. **81**(9), 941–958 (2018).
31. M. B. M. Meddens, S. Liu, P. S. Finnegan, T. L. Edwards, C. D. James, and K. A. Lidke, "Single objective light-sheet microscopy for high-speed whole-cell 3D super-resolution," Biomed. Opt. Express **7**(6), 2219–2236 (2016).
32. A. Piruska, I. Nikcevic, S. H. Lee, C. Ahn, W. R. Heineman, P. A. Limbach, and C. J. Seliskar, "The autofluorescence of plastic materials and chips measured under laser irradiation," Lab Chip **5**(12), 1348–1354 (2005).
33. P. S. Nunes, P. D. Ohlsson, O. Ordeig, and J. P. Kutter, "Cyclic olefin polymers: Emerging materials for lab-on-a-chip applications," Microfluid. Nanofluid. **9**(2-3), 145–161 (2010).

Biomedical Optics EXPRESS

34. J. S. Jeon, S. Chung, R. D. Kamm, and J. L. Charest, "Hot embossing for fabrication of a microfluidic 3D cell culture platform," Biomed. Microdevices **13**(2), 325–333 (2011).
35. J. N. Lee, C. Park, and G. M. Whitesides, "Solvent compatibility of poly(dimethylsiloxane)-based microfluidic devices," Anal. Chem. **75**(23), 6544–6554 (2003).
36. Y. Wu, A. Ghitani, R. Christensen, A. Santella, Z. Du, G. Rondeau, Z. Bao, D. Colón-Ramos, and H. Shroff, "Inverted selective plane illumination microscopy (iSPIM) enables coupled cell identity lineaging and neurodevelopmental imaging in Caenorhabditis elegans," Proc. Natl. Acad. Sci. U. S. A. **108**(43), 17708–17713 (2011).
37. P. Strnad, S. Gunther, J. Reichmann, U. Krzic, B. Balazs, G. De Medeiros, N. Norlin, T. Hiiragi, L. Hufnagel, and J. Ellenberg, "Inverted light-sheet microscope for imaging mouse pre-implantation development," Nat. Methods **13**(2), 139–142 (2016).
38. J. Girstmair, A. Zakrzewski, F. Lapraz, M. Handberg-Thorsager, P. Tomancak, P. G. Pitrone, F. Simpson, and M. J. Telford, "Light-sheet microscopy for everyone? Experience of building an OpenSPIM to study flatworm development," BMC Dev. Biol. **16**(1), 22 (2016).
39. R. M. Power and J. Huisken, "A guide to light-sheet fluorescence microscopy for multiscale imaging," Nat. Methods **14**(4), 360–373 (2017).
40. M. Born and E. Wolf, *Principles of Optics*, 7th ed. (Cambridge University Press, 1999).
41. G. De Medeiros, N. Norlin, S. Gunther, M. Albert, L. Panavaite, U. M. Fiuza, F. Peri, T. Hiiragi, U. Krzic, and L. Hufnagel, "Confocal multiview light-sheet microscopy," Nat. Commun. **6**, 1–8 (2015).
42. E. Mei, P. A. Fomitchov, R. Graves, and M. Campion, "A line scanning confocal fluorescent microscope using a cmos rolling shutter as an adjustable aperture," J. Microsc. **247**(3), 269–276 (2012).
43. E. Baumgart and U. Kubitscheck, "Scanned light sheet microscopy with confocal slit detection," Opt. Express **20**(19), 21805 (2012).
44. Z. Yang, M. Prokopas, J. Nylk, C. Coll-Lladó, F. J. Gunn-Moore, D. E. K. Ferrier, T. Vettenburg, and K. Dholakia, "A compact Airy beam light sheet microscope with a tilted cylindrical lens," Biomed. Opt. Express **5**(10), 3434 (2014).
45. T. A. Planchon, L. Gao, D. E. Milkie, M. W. Davidson, J. A. Galbraith, C. G. Galbraith, and E. Betzig, "Rapid three-dimensional isotropic imaging of living cells using Bessel beam plane illumination," Nat. Methods **8**(5), 417–423 (2011).
46. T. Meinert and A. Rohrbach, "Light-sheet microscopy with length-adaptive Bessel beams," Biomed. Opt. Express **10**(2), 670–681 (2019).
47. H. U. Dodt, U. Leischner, A. Schierloh, N. Jährling, C. P. Mauch, K. Deininger, J. M. Deussing, M. Eder, W. Zieglgänsberger, and K. Becker, "Ultramicroscopy: Three-dimensional visualization of neuronal networks in the whole mouse brain," Nat. Methods **4**(4), 331–336 (2007).
48. F. O. Fahrbach, V. Gurchenkov, K. Alessandri, P. Nassoy, and A. Rohrbach, "Self-reconstructing sectioned Bessel beams offer submicron optical sectioning for large fields of view in light-sheet microscopy," Opt. Express **21**(9), 11425 (2013).
49. O. E. Olarte, J. Andilla, D. Artigas, and P. Loza-Alvarez, "Decoupled illumination detection in light sheet microscopy for fast volumetric imaging," Optica **2**(8), 702 (2015).
50. R. McGorty, H. Liu, D. Kamiyama, Z. Dong, S. Guo, and B. Huang, "Open-top selective plane illumination microscope for conventionally mounted specimens," Opt. Express **23**(12), 16142 (2015).
51. A. Woehler, F. Preusser, J. Wisniewski, N. Vladimirov, R. A. Desai, S. Preibisch, Z. Yaniv, S. Preibisch, S. Preibisch, and S. Preibisch, "Dual-view light-sheet imaging through a tilted glass interface using a deformable mirror," Biomed. Opt. Express **12**(4), 2186–2203 (2021).